A New Nonlinear Observer for Liquid Water Estimation in Fuel Cells

Andreu Cecilia, Daniele Astolfi, Ramon Costa-Castelló

A New Nonlinear Observer for Liquid Water Estimation in Fuel Cells

Andreu Cecilia, *Member, IEEE*, Daniele Astolfi and Ramon Costa-Castelló, *Senior Member, IEEE*

***Abstract*—Fuel cells are electrochemical devices with some internal variables that cannot be measured, but have to be monitored in real-time. That is the case for the liquid water inside the fuel cell catalyst layer. This motivates the development of online algorithms, i.e. observers, able to estimate such variables. Nonetheless, fuel cell dynamics are strongly nonlinear, with significant parametric uncertainty and significant sensor noise. Therefore, typical observers, as the extended Kalman filter, usually underperform or are unstable in such systems. To overcome such limitation, this work proposes a novel nonlinear observer to estimate the liquid water saturation in fuel cells based on an inherent differential detectability of the liquid water dynamics. The stability of the proposal is formally analysed and is validated through numerical simulations and in an experimental prototype, where noise and uncertainty are considered.**

***Index Terms*—Polymer electrolyte membrane fuel cell (PEMFC), Nonlinear observer, uncertain system**

I. Introduction

Critical energy challenges have motivated the introduction and the use of hydrogen in energy systems. In this context, polymer electrolyte membrane fuel cells (PEMFC) are remarkable devices to convert the chemical energy of hydrogen into electrical energy, due to its low operating temperature, lack of moving part, zero emissions, quick start-up and high-energy density [1].

In its most basic form, a PEMFC consists of a solid polymer that is used as an electrolyte between the anode and the cathode. The fuel cell anode is constantly delivered with pure hydrogen. This hydrogen is processed at a platinum based catalyst layer, which separates the H_2 into protons and electrons. The protons travel to the cathode catalyst layer through the membrane. However, due to the membrane ionic properties, the electrons are forced to travel through an external circuit, which generates the electrical load of the device. In parallel, the cathode is feed with pure oxygen or air, which flows to the cathode catalyst layer. In this layer, the oxygen is combined with the protons to generate water and heat, which closes the overall reaction. A general scheme of the operation of a PEMFC can be found in Fig. 1.

This work has been partially funded by the Spanish Ministry of Universities funded by the European Union - NextGenerationEU (2022UPC-MSC-93823). This work is part of the Project MAFALDA (PID2021-126001OB-C31) funded by MCIN/ AEI /10.13039/501100011033 and by "ERDF A way of making Europe". This work is part of the project MASHED (TED2021-129927B-I00), funded by MCIN/ AEI/10.13039/501100011033 and by the European Union Next GenerationEU/PRTR.

A. Cecilia and R. Costa-Castelló are with the Universitat Politècnica de Catalunya, Avinguda Diagonal, 647, 08028 Barcelona, Spain (e-mail: andreu.cecilia@upc.edu and ramon.costa@upc.edu). (*Corresponding author: Andreu Cecilia*)

D. Astolfi is with the Univ. Lyon, Université Claude Bernard Lyon 1, CNRS, LAGEPP UMR 5007, Villeurbanne F-69100, France (e-mail: daniele.astolfi@univ-lyon1.fr).

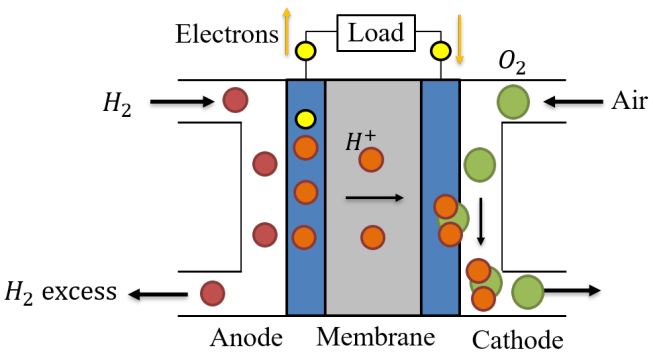

Fig. 1. General scheme of a single PEM fuel cell operation.

Although PEMFCs present promising properties, the economical viability of these devices is limited by degradation issues [2]. Indeed, fuel cell operation is related to thermal, chemical and electrical processes with internal states that will vary during the operation. Improper managing of these internal states will eventually lead to performance loss and system degradation [3]. Consequently, there is a necessity of monitoring and controlling such internal variables [4], [5].

A critical variable in PEMFCs is the water inside the device [6]. Specifically, during its operation, there is a natural generation of water in the cathode due to the reduction reaction. If too much water accumulates in the channels, the reactants cannot efficiently reach the catalyst layer, potentially leading to unstable voltages and performance losses. However, if too much water is removed and the fuel cell membrane dries out, the membrane conductivity decreases, resulting in increased ohmic losses in the system. Therefore, there is a need of monitoring the water inside the PEMFC in real-time.

However, measuring the water in real-time is not a straightforward task. Indeed, direct measurement techniques such as the current distribution method [7], neutron radiography [8], or x-ray radiography [9] are too slow and invasive to be implemented in real-time. This reality has driven the development of online water estimation algorithms. In control theory, these algorithms are often referred to as *state observers*. See, for instance, [10] for a recent survey on this topic.

The objective of this work is to develop a state observer to estimate the liquid water of a PEMFC cathode catalyst layer using easily measurable signals. This problem presents several challenges that must be taken into account. First, PEMFC dynamic models are associated with highly nonlinear processes. Typically, this challenge is addressed by approximating the system using Taylor linearization and subsequently

implementing a linear observer within the resulting linear system. This approximated approach is akin to the common extended Kalman filter (EKF), as seen in references such as [11] and [12]. Nevertheless, this linear approximation remains valid only when the observer states are initialized sufficiently close to their true values, which is often unattainable in electrochemical systems. Consequently, EKFs exhibit fragile stability properties and limited accuracy in electrochemical systems, as noted in [13]. Second, PEMFC mathematical models entail significant parametric uncertainties; that is, there are model parameters that are challenging to accurately identify. As a result, the mathematical model generally exhibits substantial discrepancies in relation to the true physical process. Observers are model-based estimation algorithms; consequently, parametric uncertainties must be considered and addressed during the observer design process. It's worth noting that this aspect has already been taken into account in some prior research, which has led to the utilization of robust observer techniques [14] and sliding-mode observers [15].

Previous studies have proposed various observers for estimating liquid water saturation in PEMFC. For example, a high-gain observer approach was introduced in [16], [17], a sliding-mode observer can be found in [18], [19], and an adaptive observer was implemented in [20]. Nevertheless, all of these works had two significant drawbacks. Firstly, the observers necessitated high-gain feedback terms, which negatively affected the transient performance of the estimator and significantly increased the algorithm's susceptibility to noise. Secondly, all of these observers required the inversion of an ill-posed matrix, which could potentially lead to numerical issues during practical implementation. An alternative estimation approach can be found in [21], where liquid water saturation is treated as a constant parameter and estimated through a robust parameter estimation algorithm. However, the accuracy of this approach may be compromised in scenarios where liquid water content varies over time.

This work proposes a new observer that solves the aforementioned limitations. The specific contributions of this work are:

- Propose a simple nonlinear observer, that exploits the differential detectability property of the system, in order to estimate the liquid water in the cathode catalyst layer of a PEMFC using only a temperature sensor.
- Include the voltage signal in the proposed observer to improve the settling time[1], the robustness in front of parametric uncertainty and the noise sensitivity of the algorithm.
- Validate the overall observer through numerical simulations and in an experimental prototype, where sensor noise and uncertainty are taken into account.

The rest of this paper is organized as follows. Section II introduces a PEMFC model that will be used to design the observer and formulates the estimation problem to be solved. Section III presents the equations of the observer. Section IV validates the proposal through a set of numerical simulations while Section V validates the technique in a real experimental prototype. Finally, some conclusions are drawn in Section VI.

[1]The settling time of the observer is defined as the time required for the observer states to reach a 5% error band around its steady-state.

II. Problem formulation

A. PEMFC model

The proposed observer is developed employing the control-oriented lumped parameter model presented and validated in [22]. This model has been used to solve multiple control problems in PEM fuel cell systems [23] and has been previously used to solve similar estimation problems [20]. Specifically, the model can be depicted in the following state-space form:

$$\begin{aligned} \dot{\mathbf{x}} &= \mathbf{f}(\mathbf{x}, I, v_{air}) \\ y_1 &= \mathbf{c}\mathbf{x} = T_{fc} \\ y_2 &= v_{fc}(\mathbf{x}, I). \end{aligned} \tag{1}$$

The state vector, $\mathbf{x}$, is defined as: $\mathbf{x} = [T_{fc}, s]^\top$, where T_{fc} $[K]$ is the temperature in the fuel cell cathode catalyst layer and s $[-]$ is the liquid water saturation in the cathode catalyst layer. The model includes two control inputs: the load current, I $[A]$, and the cathode air velocity, v_{air} $[m\ s^{-1}]$. Finally, it is assumed that that there are two measurable outputs, $[y_1, y_2]^\top$: the temperature in the cathode catalyst layer, T_{fc}, and the stack voltage v_{fc} $[V]$.

Furthermore, the function $\mathbf{f}$ is defined as:

$$\mathbf{f}(\mathbf{x}, I, v_{air}) = \begin{bmatrix} K_1(E_{ocv} n_{cell} - v_{fc})I + K_2(T_{amb} - T_{fc})v_{air} - K_{11} f_p(T_{fc}, s) \\ K_3 I - K_4 f_p(T_{fc}, s) + K_5 f_d(s) \end{bmatrix}$$

where E_{ocv} $[V]$ is the open-circuit voltage, n_{cell} $[-]$ is the number of cells, T_{amb} is the ambient temperature, the constants $K_1, .., K_5$ are defined as:

$$K_1 = \frac{1}{m_s c_{p,s}}, \quad K_2 = \frac{\rho_{air} A_{inlet} c_{p,air}}{m_s c_{p,s}}, \quad K_3 = \frac{M_{H_2O}}{2F A_{cell} K_s},$$
$$K_4 = \frac{M_{H2O} K_{evap}}{R K_s A_{pore}}, \quad K_5 = \sigma_{H_2O} \cos(\theta_{CL}) \sqrt{\varepsilon K_l^{eff}} \frac{\rho_l}{K_s \mu_l},$$
$$K_{11} = \frac{K_4 \Delta H_{vap}}{m_s c_{p,s}},$$

where m_s $[kg]$ is the overall stack mass, $c_{p,s}$ $[J\ kg^{-1}\ K^{-1}]$ is the effective stack heat capacity, ρ_{air} $[kg\ m^{-3}]$ is the air density, A_{inlet} $[m^2]$ is the inlet cross-sectional area, $c_{p,air}$ $[J\ kg^{-1}\ K^{-1}]$ is the air heat capacity, F $[C\ mol^{-1}]$ is the Faraday constant, K_s $[kg\ m^{-2}]$ is an ionomer accumulation coefficient, σ $[N\ m^{-1}]$ is the surface tension of water, K_{evap} $[m^3\ s^{-1}]$ is the evaporation time constant, A_{pore} $[m^2\ m^{-3}]$ is the effective pore surface area per unit volume, M_{H_2O} $[kg\ mol^{-1}]$ is the water molar mass, θ_{cl} $[^\circ]$ is the effective contact angle of the catalyst layer, ρ_l $[kg\ m^{-3}]$ is the liquid water density, μ_l $[kg\ m^{-1}\ s^{-1}]$ is the water dynamic viscosity and $\delta_{CL,c}$ $[m]$ is the catalyst layer width, R $[J\ K^{-1}\ mol^{-1}]$ is the ideal gas constant, ΔH_{vap} $[J\ mol^{-1}]$ is the enthalpy of vaporization.

The nonlinear functions f_p and f_d are computed as:

$$f_p(T_{fc}, s) = \frac{s}{T_{fc}}(p^0 e^{-K_6/(T_{fc})} - K_7),$$
$$f_d(s) = s(-0.96 + 3.32s - 3.78s^2).$$

where $K_6 = \dfrac{E_a}{k_b}$, with E_a $[eV]$ being the activation energy of the evaporation, the factor k_b $[eV\ K^{-1}]$ being the Boltzmann parameter, p^0 $[Pa]$ is a pre-exponential factor and K_7 $[Pa]$ being the water vapour pressure in the CCL.

Relative to the electrical side, a function that relates the states, $\mathbf{x}$, and the fuel cell output voltage, v_{fc}, is included in the model. Specifically, the voltage is computed as:

$$v_{fc}(\mathbf{x}, I) = n_{cell}(E_{ocv} - \eta_{act} - \eta_{ohm}). \tag{2}$$

The factor η_{ohm} depicts the ohmic losses which are computed through the ohm's law,

$$\eta_{ohm} = R_{ohm} I$$

where R_{ohm} $[\Omega]$ accounts for the ionic conductivity of the membrane and the resistance of the fuel cell's electric conductive components. In this work, we employ a simplifying assumption by treating the ohmic resistance, R_{ohm}, as a constant parameter. It is worth noting that the conductivity of the fuel cell membrane is known to depend on factors such as the membrane's water content and temperature, as documented in references [6, Section 2.1] and [24]. These factors can potentially vary during the operation of the fuel cell. However, adopting this assumption serves to streamline the observer design and analysis processes. Furthermore, the experimental validation presented in Section V of this paper provides empirical evidence that, even with this assumption in place, the observer still demonstrates satisfactory accuracy and performance.

Remark II.1. *It's important to distinguish between two distinct variables: the membrane water content and the liquid water saturation. The membrane water content specifically pertains to the quantity of water absorbed by the hydrophilic clusters containing $H^+SO_3^-$ in the membrane, as outlined in [6, Section 2.1]. On the other hand, the liquid water saturation relates to the volume fraction of liquid water within the porous regions of the catalyst layer and at the interface between the catalyst layer and the membrane, as detailed in [6, Section 2.3]. While these variables are interconnected—more liquid water can lead to increased water absorption by the membrane—they are not equivalent. It is essential to underscore that the primary objective of this paper is to estimate the liquid water saturation within the catalyst layer.*

Certainly, the accuracy of the observer presented in this paper may be affected by the model simplification regarding the ohmic resistance. To enhance the accuracy of the observer in real-world scenarios, it's possible to incorporate mechanisms for real-time estimation of the ohmic resistance. One approach to achieve this is by coupling the observer with a system designed explicitly for estimating the membrane water content, such as the one proposed in [25]. Once this water content estimation is obtained, the relationship between water content, temperature, and ohmic resistance, as described in [24], can be employed to estimate the ohmic resistance. Alternatively, a current interrupt strategy, as discussed in [26], can be implemented to directly acquire an estimation of the ohmic resistance. These strategies can contribute to improving the accuracy of the observer in real-world applications where the ohmic resistance varies with changing conditions. However, these strategies are out of the scope of this paper.

The factor η_{act} accounts for the activation losses which is computed as:

$$\eta_{act} = K_8 T_{fc} ln\left(\frac{I}{A_{geo} j_0(\mathbf{x})}\right)$$

where A_{geo} $[m^2]$ is the effective area of the cathode catalyst layer. The parameter K_8 is computed as

$$K_8 = \frac{R}{2\alpha F}$$

where α is the fuel cell transfer coefficient. The factor j_0 depicts the exchange current density which is computed as [23],

$$j_0(\mathbf{x}) = K_9\left(1 - \left(\frac{s_{opt} - s}{s_{opt}}\right)^{1/3}\right) e^{\left(\frac{-K_{10}}{T_{fc}}\left[1 - \frac{T_{fc}}{T_{ref}}\right]\right)}$$

where T_{ref} $[K]$ is the stack temperature at a reference operating conditions, s_{opt} $[-]$ is the liquid water saturation in which the effective electrochemically active surface area is maximum. The parameters K_9 and K_{10} are computed as

$$K_9 = j_0^{ref} a_c, \quad K_{10} = \frac{\Delta G^*}{R}$$

where j_0^{ref} $[A\ m^{-2}]$ and a_c $[-]$ are the reference exchange current and electrode rugosity, respectively, at a reference operating conditions, and ΔG^* $[J\ mol^{-1}]$ is the activation barrier for the oxygen reduction reaction on platinum.

Finally, it is important to emphasize that the states and controlled inputs of the presented fuel cell model are assumed to be bounded, positive, and non-zero. Otherwise, the studied fuel cell system could encounter severe degradation and security issues. Consequently, the model states, denoted as $\mathbf{x}$, are expected to evolve within a compact set $\mathcal{X} \subset \mathbb{R}^2$, while the controlled inputs, represented as (v_{air}, I), are defined within another compact set $\mathcal{U} \subset \mathbb{R}^2$. For this work, we assume that the fuel cell operates within the region where $I > 0$, $v_{air} > 0$, $T_{fc} > 0$, and $s_{opt} > s > 0$.

B. Main Objectives

The primary objective is to design an observer that utilizes the information from the measured outputs, T_{fc} and v_{fc}, as well as the control inputs I and v_{air}, to generate an estimation of the states, denoted as $\hat{\mathbf{x}}$. This estimation should converge asymptotically to zero, meaning we aim for the following condition to hold:

$$\lim_{t\to\infty} |\mathbf{x}(t) - \hat{\mathbf{x}}(t)| = 0. \tag{3}$$

There are multiple techniques that can be employed to address this problem. However, to design an observer suitable for practical implementation, it's crucial to consider the presence of unmodeled elements during the observer design phase. In particular, fuel cell sensors typically exhibit a significant amount of sensor noise. Moreover, due to the challenges associated with measuring fuel cell liquid water saturation,

identifying parameters related to liquid water dynamics is a formidable task. Therefore, it's reasonable to assume that significant parametric uncertainty will be associated with the parameters $K_i,\ \forall i \in 3,..,7$. Naturally, in the presence of such unmodeled elements, achieving the objective outlined in (3) becomes unattainable. Instead, we can only ensure practical convergence, denoted as $\lim_{t\to\infty} |\hat{\mathbf{x}}(t) - \mathbf{x}(t)| \leq \varepsilon$, where ε is a positive constant. Consequently, the proposed observer must minimize the impact of sensor noise and parametric uncertainty on the quality of the estimation.

III. Observer proposal

A. Observer Dynamics

Considering the strong nonlinear nature of the model dynamics, it is advantageous to design a nonlinear observer by directly analyzing the dynamics of the PEMFC model. This approach avoids relying on approximations based on Taylor linearization [27], [28]. Such approximations typically lead to local observers, where the observer states must be initialized "close enough" to the true values to ensure that the Taylor linearization adequately approximates the model, as discussed in detail in [11]. Notably, in PEMFC systems, accurately determining the value of liquid water saturation is particularly challenging, rendering such initialization unfeasible. Therefore, this work introduces a nonlinear observer capable of accurately estimating the states of the PEMFC system, regardless of the observer's initial conditions. For a more comprehensive exploration of nonlinear observer design for general nonlinear systems, readers are directed to [10].

An interesting property of the studied model is that the system is differentially detectable with respect to a constant metric $\mathbf{P} \in \mathbb{R}^{2\times 2}$ taking the stack temperature, y_1, as the measured output. For an introduction to the concept of differential detectability with constant metrics and its connection to the classical notion of detectability, we refer the reader to Appendix A.

Precisely, for any value $K_3, K_4, K_5, K_6, K_7 > 0$, there exists a positive definite symmetric matrix $\mathbf{P}$ and some positive constants q and μ such that

$$\mathbf{P}\frac{\partial \mathbf{f}}{\partial \mathbf{x}}(\mathbf{x}, I, v_{air}) + \frac{\partial \mathbf{f}}{\partial \mathbf{x}}(\mathbf{x}, I, v_{air})^\top \mathbf{P} - \mu \mathbf{c}^\top \mathbf{c} \leq -q\mathbf{P}. \quad (4)$$

for all $(\mathbf{x}, I, v_{air}) \in \mathcal{X} \times \mathcal{U}$, where $\mathbf{c} = [1\ 0]$. The proof that such condition is satisfied can be found in Appendix B. The reader is also referred to [10, Section 4], [29], [30] for a formal definition of differential detectability and its use in observer design. In practice, differential detectability can be understood as a nonlinear extension of the classical notion of detectability of linear systems.

The main advantage of differential detectability is that, it can be shown (see [10, Section 4]) that the following observer

$$\dot{\hat{\mathbf{x}}} = \mathbf{f}(\hat{\mathbf{x}}, I, v_{air}) + \kappa \mathbf{P}^{-1}\mathbf{c}^\top (y_1 - \mathbf{c}\hat{x}) \quad (5)$$

satisfies the condition (3) in all $\mathcal{X}$, namely, independently of the initial conditions of the plant and observers. In (5), $\mathbf{P}$ is the matrix computed in (4) and κ is a positive parameter to be chosen large enough. The formal proof of such a statement is included in Appendix C.

B. Comparison with Extended Kalman Filter

The presence of the Jacobian of the function $\mathbf{f}$ in (4) and the structure of the observer in (5) bears a resemblance to the deterministic Extended Kalman Filter (EKF) [11], [12], [31]. However, there are some significant differences that need to be taken into consideration. In the system under consideration, the deterministic EKF exhibits the following structure

$$\begin{aligned}\dot{\hat{\mathbf{x}}} &= \mathbf{f}(\hat{\mathbf{x}}, I, v_{air}) + \mathbf{P}_{KF}\mathbf{c}^\top R^{-1}(y_1 - \mathbf{c}\hat{\mathbf{x}}) \quad (6)\\ \dot{\mathbf{P}}_{KF} &= \frac{\partial \mathbf{f}}{\partial \mathbf{x}}(\hat{\mathbf{x}}, I, v_{air})\mathbf{P}_{KF} + \mathbf{P}_{KF}\frac{\partial \mathbf{f}}{\partial \mathbf{x}}(\hat{\mathbf{x}}, I, v_{air})^\top + \mathbf{Q}\\ &\quad - \mathbf{P}_{KF}\mathbf{c}^\top R^{-1}\mathbf{c}\mathbf{P}_{KF},\end{aligned}$$

with $R = R^\top > 0$ and $\mathbf{Q} = \mathbf{Q}^\top > 0$ being matrices to be tuned. The main differences between the proposed observer in (5) and the EKF (6) are summarized in the following list.

- The matrix $\mathbf{P}$ in (5) remains constant, whereas the matrix $\mathbf{P}_{KF}$ in the EKF (6) is time-varying. Analyzing the transient behavior of an observer with a constant feedback term is much simpler compared to observers with time-varying gains.
- The stability of the EKF (6) necessitates the existence of constants $\underline{p}, \overline{p} > 0$ such that [11], [12], [31]

  $$\underline{p} I \leq \mathbf{P}_{KF}(t) \leq \overline{p} I, \quad \forall t. \quad (7)$$

  However, the trajectory of $\mathbf{P}_{KF}$ depends on the value of the observer state $\hat{\mathbf{x}}$. Therefore, the assumption in (7) introduces a loop in the observer analysis, which can only be resolved by imposing additional conditions on the system and ensuring that $\mathbf{x} - \hat{\mathbf{x}}$ is initially small enough. This is why the EKF (6) is considered a local observer and requires initializing the observer states close to their true values. On the other hand, the proposed observer in (5) does not involve this analysis loop, is global, and does not demand precise initialization.
- The proposed observer in (5) has a dimension of 2 and only requires tuning a single matrix, $\mathbf{P}$. In contrast, the Extended Kalman Filter is of dimension 4 and involves tuning two matrices, $\mathbf{Q}$ and R.
- The Extended Kalman filter does not leverage the advantageous property of differential detectability (4).

For these reasons, this work has found it more convenient to implement the observer in (5) than the more common EKF (6).

C. Limitations of the proposal

While the previous subsection has highlighted some benefits of the proposed observer, it is important to acknowledge that the proposal is not without drawbacks. Primarily, since the observer is based on a detectability assumption, the settling time of the observer cannot be arbitrarily adjusted and depends on the system dynamics. As liquid water dynamics are relatively slow, typically taking around 100-1000 seconds to reach a steady state [6], the observer's convergence is also relatively slow. Additionally, the detectability assumption (4) in the proposed observer implies that the observer is sensitive to parametric uncertainty in the liquid water equation dynamics. In other

words, small uncertainties in the parameters $K_i,\ \forall i \in 3,..,7$, can lead to significant estimation errors, and these errors cannot be mitigated through observer tuning. It's worth noting that this drawback also applies to an EKF. Moreover, it's important to highlight that, as mentioned in Subsection II-B, a significant amount of parametric uncertainty is expected in the liquid water dynamics, making this drawback particularly critical. A more detailed explanation is provided at the end of Appendix C. For a more in-depth analysis of the relationship between detectability, settling time, and robustness for generic nonlinear systems, readers are encouraged to refer to [32].

These limitations render the proposed observer (4) impractical for implementation. However, there exists a straightforward modification that addresses the aforementioned settling time and parametric sensitivity issues. The next subsection will concentrate on introducing this modification.

D. Observer improvement by adding the voltage signal

An interesting design choice is that the observer (5) does not incorporate the voltage signal $y_2 = v_{fc}(\mathbf{x}, I)$. Intuitively, incorporating additional sensor information could enhance the quality of the observer's estimation. Therefore, in this work, we investigate the possibility of leveraging the voltage sensor to address the limitations of the observer (5).

It should be noted that, in general, there is no established methodology for integrating additional sensors into already designed nonlinear observers. In other words, designing nonlinear observers when dealing with multiple outputs is a challenging task, and there is no universal approach to solve this problem. However, the voltage equation under consideration exhibits a property that is particularly advantageous for this task. Specifically, the voltage equation is monotonic with respect to the liquid water saturation, s. That is, for any T_{fc}, s and I in the considered operating region, the following is satisfied

$$(s - \hat{s})\big[v_{fc}(\mathbf{x}, I) - v_{fc}(\mathbf{x}', I)\big] \geq |s - \hat{s}|^2, \tag{8}$$

where $\mathbf{x}' = [T_{fc},\ \hat{s}]$. Monotonicity has a clear interpretation. Specifically, the voltage value increases whenever the liquid water saturation, s, also increases, and vice-versa.

This work proposes to exploit the monotonic condition in (8) to include the voltage signal in the observer (5). Specifically, the observer in (5) is modified as follows

$$\begin{aligned}\dot{\hat{\mathbf{x}}} = \mathbf{f}(\hat{\mathbf{x}}, I, v_{air}) + \kappa \mathbf{P}^{-1}\mathbf{c}^\top(y_1 - \mathbf{c}\hat{\mathbf{x}}) \\ + \rho \mathbf{P}^{-1}\begin{bmatrix}0\\1\end{bmatrix}(y_2 - v_{fc}(\mathbf{x}', I)),\end{aligned} \tag{9}$$

where $\mathbf{P}$ is a constant matrix that satisfies (4), ρ and κ are parameters to be tuned and $\mathbf{x}' = [y_1,\ \hat{s}]$. As shown in Appendix D, the observer (9) is an asymptotic observer for the plant (1) satisfying the condition (3).

Introducing the second term in (9) leads to a significant reduction in the settling time of the observer and decreases its sensitivity to parametric uncertainty in the parameters $K_i,\ \forall i \in 3,..,7$, all without increasing the dimension of the observer or introducing additional parameters to be tuned. A proof of this assertion is provided at the end of Appendix D. Furthermore, the enhancement in the observer's performance will be validated through numerical simulations in Section IV.

IV. Numerical Simulations

The viability and advantages of the proposed observer (9) were initially validated through a series of numerical simulations. In the first set of simulations, we compared the performance of the observer in (9) with that of the observer in (5) under various case scenarios. In the final simulation, we compared the performance of the observer in (9) with that of the EKF in (6).

In all case scenarios, a fuel cell digital twin modelled through the equations in (1) and the parameters in Table II of Appendix E (Value (simulation) column) will be excited with a periodic current profile that oscillates between $5\ A$ and $3.8\ A$, and a constant cathode air velocity, $v_{air} = 0.9$. Consequently, the model will generate some signals T_{fc} and v_{fc} that will be used in the observers to generate an estimation of the liquid water saturation, $\hat{s}$. To assess the quality of the estimation, the signal $\hat{s}$ generated by the observer will be contrasted with the true value of the liquid water saturation, s, generated by the digital twin. In all case scenarios, the observer parameters have been fixed to an arbitrary value $\kappa = \rho = 1$. The matrix $\mathbf{P}$ has been selected as $\mathbf{P} = \begin{bmatrix}2 & 1\\ 1 & 1\end{bmatrix}$, which satisfies the condition in (4). Further details on how to tune the matrix $\mathbf{P}$ are included in Appendix B.

A. Case scenario 1: Perfect model and sensors without noise

In the first case scenario, we assume that the equations of the observer share the same model parameters as the digital twin responsible for generating the measured signals. In other words, the factor $\mathbf{f}(\hat{\mathbf{x}}, I, v_{air})$ in the observers is implemented using the parameters from Table II (Value (simulation) column). Additionally, we assume that the sensors can provide perfect measurements of the system. Consequently, the measured signals, y_1 and y_2, remain unaffected by measurement noise.

The results of the simulation are illustrated in Fig. 2. As observed, both observers converge to the true value. However, the observer in (5) exhibits a relatively lengthy settling time, requiring approximately 30 seconds to converge. This can be attributed to two factors. First, the settling time of the observer in (5) cannot be adjusted. Second, the liquid water dynamics are relatively slow. Conversely, the observer in (9) achieves convergence significantly faster, taking only 15 seconds to settle.

It should be remarked that, as discussed before, the settling time of the observer in (5) cannot be reduced by increasing or decreasing the factor κ. Nonetheless, the settling time of the observer in (9) can be reduced by increasing ρ.

B. Case scenario 2: Perfect model and sensors with noise

In the second case scenario, we once again assume that the factor $\mathbf{f}(\hat{\mathbf{x}}, I, v_{air})$ in the observers is implemented with the parameters from Table II, meaning that the observers utilize a perfect model with no parametric uncertainty. However, in this scenario, we assume that the sensors are not perfect. More precisely, the measured temperature is subject to white noise with a variance of 0.05, and the measured voltage is affected by white noise with a variance of 0.001.

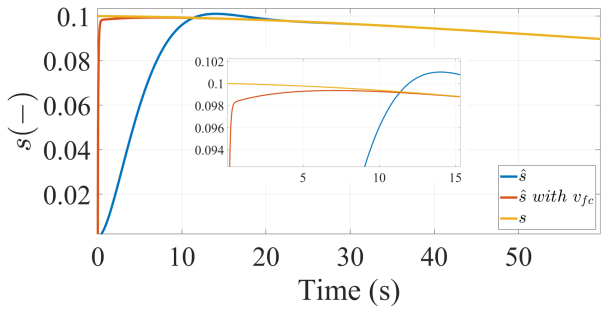

Fig. 2. Evolution of the model liquid water saturation (s), estimation of the observer in (5) ($\hat{s}$) and estimation of the observer with the voltage signal in (9) ($\hat{s}$ with v_{fv}). In both observers, the tunable parameters have been fixed at $\kappa = \rho = 1$.

The results of the simulation are illustrated in Fig. 3. The observer in (5) converges to an error with a variance of $1.0338 \cdot 10^{-4}$, whereas the observer in (9) converges to an estimation error with a variance of $6.9139 \cdot 10^{-7}$, which is approximately 150 times smaller. Remarkably, it can be concluded that incorporating the noisy voltage signal into the observer significantly reduces the impact of sensor noise on the quality of the estimation.

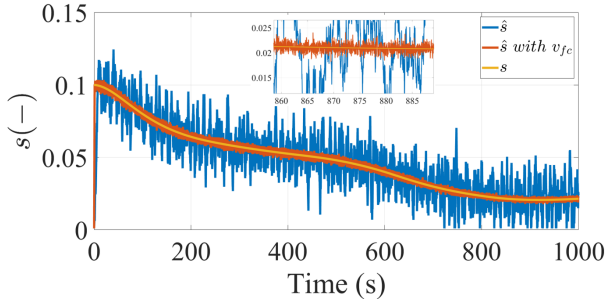

Fig. 3. Evolution of the model liquid water saturation (s), estimation of the observer in (5) ($\hat{s}$) and estimation of the observer with the voltage signal in (9) ($\hat{s}$ with v_{fc}). In both observers, the tunable parameters have been fixed at $\kappa = \rho = 1$. This simulation takes into account the presence of sensor noise.

C. Case scenario 3: Model with parametric uncertainty

In the third case scenario, we assume that the sensors are free of noise. However, in this scenario, we introduce parametric uncertainty into the models. Specifically, while the fuel cell digital twin is implemented with the parameters from Table II, the factor $\mathbf{f}(\hat{\mathbf{x}}, I, v_{air})$ in the observers is implemented with parameters K_3, K_4, K_5, K_6, and K_7 as detailed in Table I. It's important to note that the parametric uncertainty ranges from a minimum of a 10% relative error[2] to a maximum of 50%.

The results of this third simulation are depicted in Fig. 4. It can be seen that the observer in (5) converges to a relative error of around 85%, and the observer in (9) converges to a relative error of around 14%. This result confirms that adding the voltage signal reduces the sensitivity of the observer in front of parametric uncertainty.

[2]The relative error is computed as $\dfrac{|x - \hat{x}|}{x} \cdot 100\ (\%)$.

TABLE I
PARAMETERS OF THE DIGITAL TWIN MODEL AND OBSERVER

Parameter	Value (DT)	Value (Observer)	Rel. Error (%)
K_3	$2.37 \cdot 10{-}5$	$2.137 \cdot 10^{-5}$	9.83
K_4	$5.33 \cdot 10^{-5}$	$4.79 \cdot 10^{-5}$	10.13
K_5	$1.218 \cdot 10^{-4}$	$6.09 \cdot 10^{-5}$	50
K_6	5210	4429	14.99
K_7	2380	1904	20

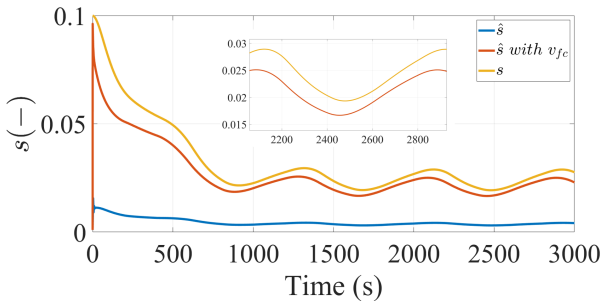

Fig. 4. Evolution of the model liquid water saturation (s), estimation of the observer in (5) ($\hat{s}$) and estimation of the observer with the voltage signal in (9) ($\hat{s}$ with v_{fc}). In both observers, the tunable parameters have been fixed at $\kappa = \rho = 1$. This simulation takes into account the presence of parametric uncertainty.

D. Case scenario 4: Comparison with the EKF

In the last case scenario, the proposed observer in (9) is compared with a set of EKFs of the form (6). This simulation considers the sensor noise presented in the Case scenario 2 and the parametric uncertainty in the Case scenario 3. In this simulation, two different parameter tunings for the EKF are considered. The first, denoted as EKF 1 in Fig. 5, is tuned with $\mathbf{Q} = \begin{bmatrix} 10 & 0 \\ 0 & 0.1 \end{bmatrix}$, $R = 0.1$. The second, denoted as EKF 2 in Fig. 5, is tuned with $\mathbf{Q} = \begin{bmatrix} 10 & 0 \\ 0 & 0.1 \end{bmatrix}$, $R = 100$.

The results of the simulation are depicted in Fig. 5. It can be seen that the EKF 1, presents larger noise sensitivity as the observer in (9), and presents significant bias during the steady-state due to the model uncertainty. In the EKF 2, the value of R has been tuned to reduce the effect of the sensor noise. In Fig. 5 it can be seen that this tuning reduces the noise sensitivity of the algorithm, but, increases the bias generated by the model uncertainty.

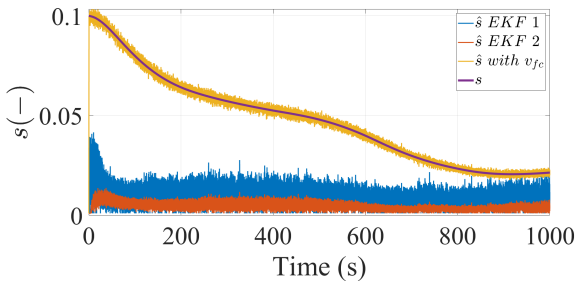

Fig. 5. Evolution of the model liquid water saturation (s), estimation of the observer in (9) ($\hat{s}$ with v_{fc}) and estimation of two EKFs. This simulation takes into account the presence of parametric uncertainty and sensor noise.

V. Experimental Validation

A. Experimental Set-up

The proposed observer has been validated in an experimental prototype. The setup features a PEMFC stack model H-100. In the setup, air is delivered to the PEMFC cathode through a fan that controls the air velocity, v_{air}. The air velocity is measured using a hot film sensor model EE75 from E+E Elektronik, and the fan is controlled using a National Instruments NI-9505 PWM module. On the anode side, a compressed hydrogen cylinder provides pure hydrogen. The setup eliminates the need for a flow controller, thus allowing the PEMFC to operate in dead-end mode [33]. This means that a pressure regulator maintains the anode inlet at 0.4 bar, and periodically, a 500 ms purge is introduced into the anode. It's worth noting that these purges introduce periodic disturbances in the measured voltage signal, as evident in Fig. 7, where periodic downward 'spikes' are observed in the voltage signal.

As the fuel cell is fed with ambient air (open-cathode architecture), the system is very sensitive to ambient conditions. Consequently, to make the experiments reproducible and repeatable, the system is enclosed in an environmental chamber that regulates oxygen concentration, humidity, and temperature.

The temperature of each cell of the stack is measured by means of a type K thermocouple. The temperature of the stack, T_{fc}, is taken as the average temperature measured in each cell.

The exchange current can be modified through a programmable load that emulates some external energy demand. Finally, an isolation amplifier AD215 from Analog Devices is used to measure the stack voltage, v_{fc} and a Hall effect sensor model LTS 6 NP is implemented to measure the exchange current.

A scheme of the set-up and a photography can be found in Fig. 6.

B. Experiment 1: Methodology

In the first experiment, the fuel cell system is excited using a specific input signal to generate the output signals utilized in the observer. More precisely, a constant exchange current, I, of $3.95\ A$, is applied to the fuel cell. Additionally, a step change in cathode air velocity, v_{air}, is introduced, transitioning from 0.21 to 0.19 by adjusting the fan input. This step change induces variations in the fuel cell stack temperature, T_{fc}, and voltage, v_{fc}, which are subsequently used in the observer to estimate the unknown liquid water saturation, s.

The fuel cell model parameters have been identified in the proposed experimental set-up and are summarized in Table II (Value (exp.) column). It should be mentioned that, as the liquid water cannot be measured, the parameters related to the water dynamics, K_3, K_4, K_5, K_6 and K_7, may have not been accurately identified. Nonetheless, as discussed in Section IV, the proposed observer presents low sensitivity to uncertainty in these parameters.

A challenge in validating the proposed observer arises from the absence of real-time liquid water sensors capable of measuring this variable. Consequently, the observer's estimation cannot be directly compared with any measured signal. To address this limitation, the following methodology will be employed. Firstly, for an initial validation, the temperature and voltage estimations generated by the observer will be compared with the actual measured signals. If the error between the estimation and measurement is low, and assuming the model is correct, we can reasonably infer that the liquid water estimation is also accurate. Secondly, for a secondary validation, the water estimation produced by the proposed observer in (9) will be compared with the water estimation generated by the experimentally validated observer in [18]. If both observers converge to similar values, then it can be concluded that the proposed observer is providing accurate estimations.

Finally, to evaluate the advantages of the proposed method compared to alternatives in the literature, the estimation from the observer (9) will be compared to the one presented in [18], which is based on a chattering-free higher-order sliding-mode approach, as well as the extended Kalman Filter discussed in Section III.

C. Experiment 1: Results and Discussion

The main results of the experimental validation are summarized in Fig. 7. First, subfigures a) and b) of Figure 7 show that the proposed observer rapidly converge to a relative error of 0.05% in the voltage signal and 0.005% in the temperature signal. Consequently, if we assume that the model is accurate, the liquid water saturation estimation in subfigure c) of Fig. 7 has to be also accurate. Second, subfigure c) compares the estimation of the proposed observer and the one presented in [18]. It can be seen that both observers converge (at around $1400\ s$) to a similar value, therefore, the accuracy of the proposed observer is similar to the one of state-of-art algorithms in the literature. These results validate the estimation quality of the observer in a practical scenario.

In addition, the primary benefit of the proposed method becomes evident when comparing the transient behavior of the observer (9) with that of the observer in [18]. In all subfigures of Fig. 7, it can be observed that both observers exhibit similar noise sensitivity. However, the settling time of the proposed observer is significantly superior. Specifically, while the observer in [18] requires approximately 1400 seconds to converge, the proposed observer converges in around 10 seconds. This outcome holds particular significance in the considered experiment, as the slow convergence of the observer in [18] hinders the ability to observe the effect of the air velocity step on the liquid water saturation. Nevertheless, when examining the estimation of the proposed observer in subfigure c), the impact of the air velocity change becomes clearly evident at around 320 seconds.

Finally, the infeasibility of the EKF in the proposed experimental setup is evident in subfigures a) and c). Specifically, the EKF yields estimations of the liquid water saturation and voltage that differ significantly from those of the proposed observer and the observer in [18]. This difference can be attributed mainly to the local nature of the EKF and the fact that the observer was initialized far from the true value of the states, preventing robust convergence of the observer.

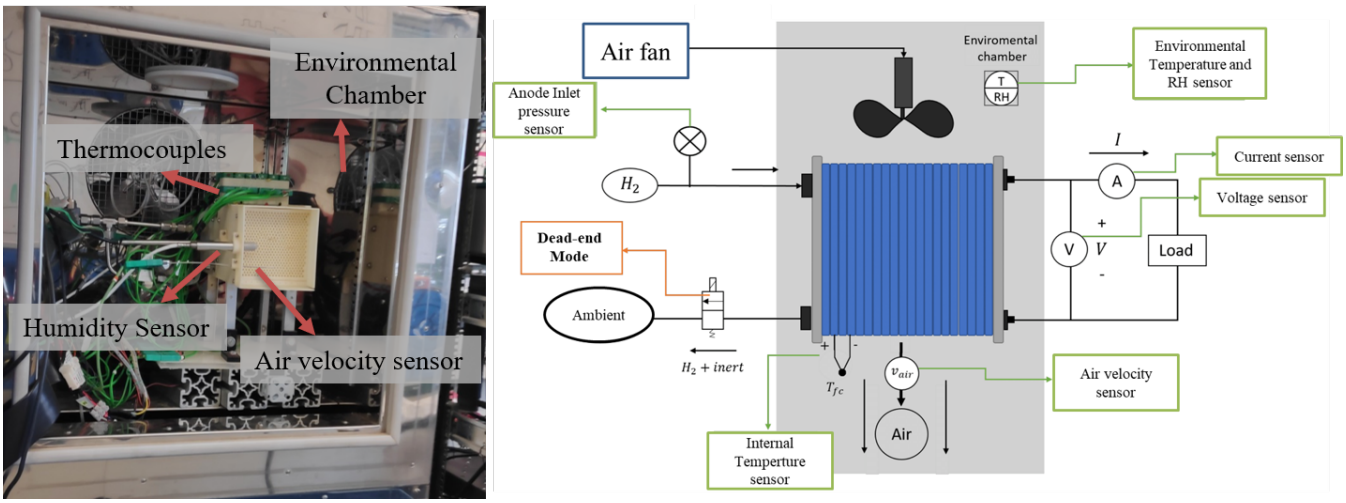

Fig. 6. (a) Environmental chamber and H-100 PEMFC. (b) H-100 experimental set-up scheme.

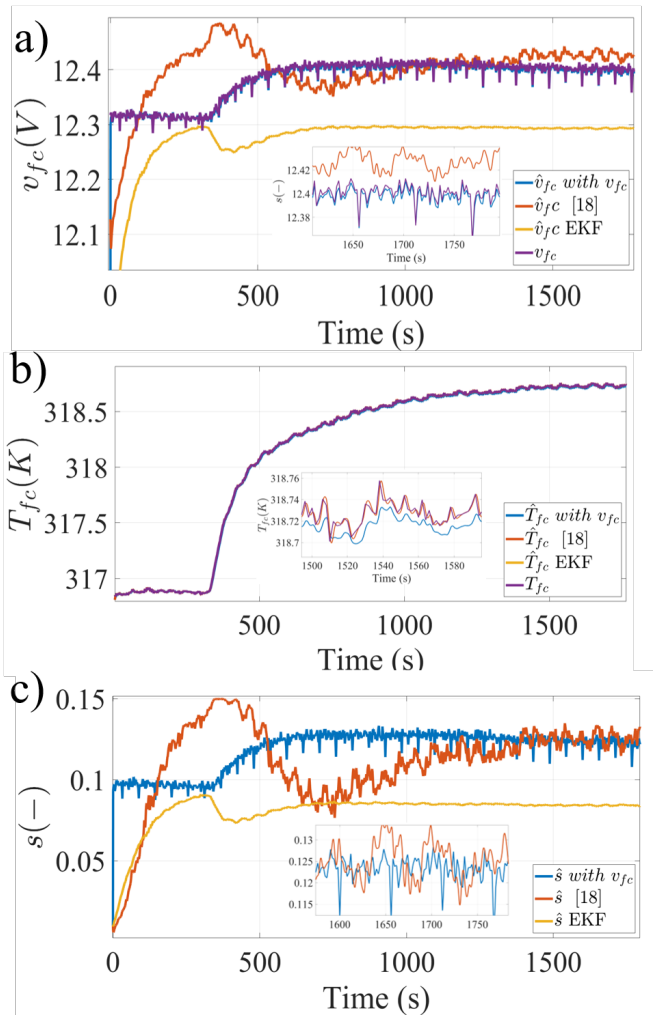

Fig. 7. a) Trajectory data of the measured stack voltage, estimation the proposed observer in (9) and estimation of the observer proposed in [18] and estimation of the EKF. b) Trajectory data of the measured stack temperature, estimation the proposed observer in (9), estimation of the EKF and estimation of the observer proposed in [18]. c) Liquid water saturation estimation of the observer proposed in [18], the EKF and estimation of the proposal in (9).

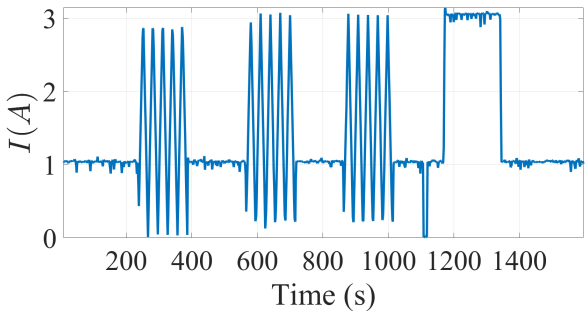

Fig. 8. Exchange current signal in the second experiment.

D. Experiment 2: Methodology

Note that the first experiment only provides data at two operating points with a small change in the cathode air velocity. In this context, the error of the EKF could potentially be reduced by (somehow) correctly initializing the observer close to these operating points. However, this is no longer applicable in the second experiment discussed in this section. Specifically, in the second experiment, the fuel cell is excited with a constant air velocity of 0.918, and the exchange current profile is depicted in Fig. 8. It should be noted that in this case, the current exhibits large oscillations of low frequencies and three set-point changes towards the end of the experiment. Consequently, any linear approximation around an equilibrium point of the fuel cell dynamics would be entirely incorrect.

This second experiment will implement the same model parameters and validation methodology as the first experiment in order to compare the proposed observer (9) and the EKF in (6).

E. Experiment 2: Results and Discussion

The main results of the second experimental validation are summarized in Fig. 9. First, subfigures a) and b) demonstrate, once again, that the proposed observer (9) rapidly converges to

a low relative error in the voltage signal and the temperature signal. Consequently, if we assume that the model is accurate, the estimation of liquid water saturation in subfigure c) should also be accurate.

Moreover, in subfigure c), noteworthy differences emerge in the liquid water estimation between the proposed observer (9) and the EKF in (6). However, upon closer examination of the voltage estimation in subfigure b, it becomes evident that the EKF estimation is fundamentally flawed.

Firstly, in the final 400 seconds of subfigure b), we observe that the proposed observer provides a voltage estimation with a relatively small error, while the EKF (9) exhibits an apparent bias. This bias can be attributed to the fact that during the last 400 seconds, the EKF generates a liquid water estimation with a smaller value compared to the one produced by the proposed observer (9). This observation validates that the proposal offers an estimation that aligns more coherently with the measured data.

Secondly, at the 1200-second mark, there is a sudden drop in the voltage, caused by an increase in the exchange current and its corresponding ohmic losses, as depicted in Fig. 8. Subsequently, there is a gradual rise in the measured voltage due to the generation of liquid water. This behaviour results from the increase in the reduction reaction, which humidifies the device and reduces the activation losses of the fuel cell. As illustrated in subfigure c), the proposed observer (9) exhibits this behaviour of increasing the liquid water saturation. Consequently, the estimated voltage also experiences a gradual increase following the sudden current increase. In contrast, the EKF's liquid water estimation fails to follow this trend, resulting in its voltage estimation not increasing accordingly.

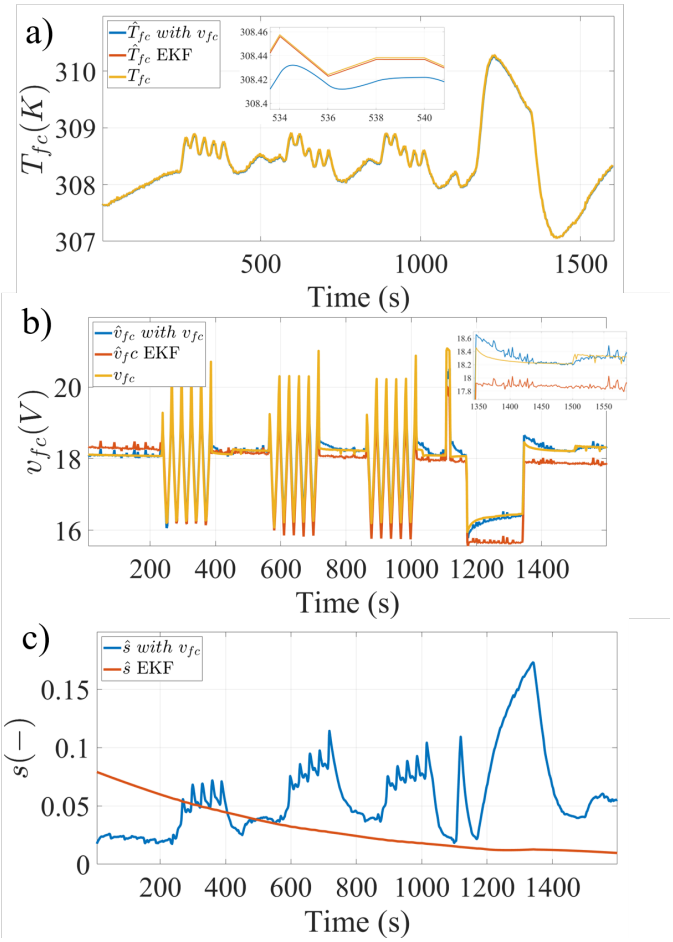

Fig. 9. a) Trajectory data of the measured stack voltage, estimation the proposed observer in (9) and estimation of the EKF. b) Trajectory data of the measured stack temperature, estimation the proposed observer in (9) and estimation of the EKF. c) Liquid water saturation estimation of the EKF and estimation of the proposal in (9).

VI. Conclusions

This work has presented a nonlinear observer for estimating the liquid water saturation in the cathode catalyst layer of PEM-FCs. It has been demonstrated that the liquid water dynamics satisfy a specific differential detectability property that can be leveraged to design a straightforward observer. Furthermore, it has been shown that by exploiting a monotonic condition from the voltage equation, the settling time and parametric sensitivity of the observer can be significantly improved. The proposed observer has been validated through numerical simulations and in an experimental prototype. Additionally, the proposal has been compared with the EKF through numerical simulations and has been experimentally compared with the state-of-the-art observer proposed in [18] and the classical EKF.

Appendix A
On differential detectability

Consider a generic plant described by finite-dimensional continuous-time dynamics of the form

$$\dot{\mathbf{x}} = \mathbf{f}(\mathbf{x}, \mathbf{u}), \quad \mathbf{y} = \mathbf{C}\mathbf{x}, \tag{10}$$

where $\mathbf{x} \in \mathbb{R}^{n_x}$ is the state, $\mathbf{y} \in \mathbb{R}^{n_y}$ is the measured output and $\mathbf{u} \subset \mathcal{U} \in \mathbb{R}^{n_u}$ are (known) inputs, where $\mathcal{U}$ is a compact set. We assume that $\mathbf{f}$ is sufficiently regular. Additionally, and driven by the practical application of the paper, we only consider solutions which we know that evolve in a certain compact set X_0.

Assumption 1. *The system* (10) *is forward invariant in a compact set $X_0 \subset \mathbb{R}^n$ uniformly in all $\boldsymbol{u} \in \mathcal{U}$.*

Naturally, we restrict ourselves to initial conditions of (10) in $X_0 \subset \mathbb{R}^{n_x}$.

In this section, we are interested in the concept of the *differential detectability* for a constant metric case as studied in [34] (see also [29] for the Riemannian metric case). This concept is formalized through the following definition.

Definition 1. *The system* (10) *is differentially detectable (with constant metric) if there exists a positive definite symmetric matrix $\boldsymbol{P} \in \mathbb{R}^{n_x \times n_x}$ some positive constants $q, \mu > 0$ such that*

$$\boldsymbol{P}\frac{\partial \boldsymbol{f}}{\partial \boldsymbol{x}}(\boldsymbol{x}, \boldsymbol{u}) + \frac{\partial \boldsymbol{f}}{\partial \boldsymbol{x}}(\boldsymbol{x}, \boldsymbol{u})^\top \boldsymbol{P} - \mu \boldsymbol{c}^\top \boldsymbol{c} \leq -q\boldsymbol{P}. \tag{11}$$

for all $\boldsymbol{x} \in X_0$ and $\boldsymbol{u} \in \mathcal{U}$.

To better understand the consequences derived from differential detectability and its link to the classical notion of detectability, consider now two solutions $\mathbf{x}, \mathbf{x}' \in X_0$ of (10)

with the same input $\mathbf{u} \in \mathcal{U}$ and define the difference between these trajectories as $\tilde{\mathbf{x}} := \mathbf{x}' - \mathbf{x}$. Moreover, consider that by means of the mean value theorem for vector valued mappings, we have the following identity

$$\dot{\tilde{\mathbf{x}}} = \mathbf{f}(\mathbf{x}, \mathbf{u}) - \mathbf{f}(\mathbf{x} - \tilde{\mathbf{x}}, \mathbf{u}) = \left(\int_0^1 \frac{\partial \mathbf{f}}{\partial \mathbf{x}}(\mathbf{x} + (s-1)\tilde{\mathbf{x}}, \mathbf{u}) ds \right) \tilde{\mathbf{x}}. \tag{12}$$

With this in mind, the inequality in (11) establishes that solutions to

$$\dot{\mathbf{x}} = \mathbf{f}(\mathbf{x}, \mathbf{u}), \quad \dot{\tilde{\mathbf{x}}} = \left(\int_0^1 \frac{\partial f}{\partial \mathbf{x}}(\mathbf{x} + (s-1)\tilde{\mathbf{x}}, \mathbf{u}) ds \right) \tilde{\mathbf{x}}$$

with $\mathbf{x}, \mathbf{x}'$ initialized at X_0 and verifying $\mathbf{C}\tilde{\mathbf{x}}(t) = 0$ satisfy [34],

$$\lim_{t \to \infty} |\tilde{\mathbf{x}}(t)| = 0. \tag{13}$$

Indeed, equation (13) is strongly related to the notion of detectability. Hence, the name differential detectability. Precisely, consider any pair of solutions $\mathbf{x}, \mathbf{x}' \in X_0$ of (10) with the same input $\mathbf{u} \in \mathcal{U}$ giving the same output **y= Cx=Cx'**. That is, consider any two trajectories indistinguishable from the output. Notice that these two trajectories satisfy the condition $\mathbf{C}\tilde{\mathbf{x}} = 0$. Therefore, differential detectability and (13) imply that indistinguishable trajectories converge asymptotically one to the other, thus, the system is detectable.

In summary, differential detectability (with constant metric) can be used as a tool to analyse the detectability of a nonlinear system. Additionally, as the next appendices will show, this property can also be used to directly design an observer.

Remark A.1. *We emphasize that differential detectability only implies that any pair of trajectories that are indistinguishable from the output will converge to each other. However, it does not provide any insight into the existence or non-existence of such indistinguishable pairs. Therefore, this property does not guarantee observability of the states.*

Remark A.2. *It is noteworthy that the Jacobian of the vector field is utilized in the definition of differential detectability. However, it's important to clarify that differential detectability is not reliant on system linearization around any specific equilibrium point or trajectory. Consequently, the property of differential detectability is global in nature, meaning that the system will exhibit detectability for any trajectory that stays within X_0, and there are no constraints preventing $X_0 \subseteq \mathbb{R}^{n_x}$.*

APPENDIX B
DIFFERENTIAL DETECTABILITY OF THE FUEL CELL MODEL

For the considered measured output equation, any constant $\boldsymbol{\delta}_x = [0 \quad \boldsymbol{\delta}_x']^\top$ satisfies the condition $\boldsymbol{\delta}_x^\top \mathbf{c}^\top \mathbf{c} \boldsymbol{\delta}_x = 0$. Now, consider a constant symmetric matrix $\mathbf{P} \in \mathbb{R}^{2\times 2}$ partitioned as

$$\mathbf{P} = \begin{bmatrix} p_1 & p_2 \\ p_2 & p_3 \end{bmatrix}. \tag{14}$$

Then, the inequality in (4) reduces to

$$\begin{aligned} \boldsymbol{\delta}_x' \Big[& 2p_2((K_{11}(K_7 - p^0 \exp(-K_6/x_1)))/x_1 \\ & + (IK_1K_8 n_{cell} x_1)/(3s_{opt}(((s_{opt} - x_2)/s_{opt})^{1/3} - 1) \\ & * ((s_{opt} - x_2)/s_{opt})^{2/3})) - 2p_3(K_5((189x_2^2)/50 \\ & - (83x_2)/25 + 24/25) \\ & + K_5 x_2((189x_2)/25 - 83/25) \\ & - (K_4(K_7 - p^0 \exp(-K_6/x_1)))/x_1) \Big] \boldsymbol{\delta}_x' < 0. \end{aligned}$$

It should be remarked, that the term multiplying the factor p_2 is always negative for the operating region $I > 0, T_{fc} > 0$ and $0 < s < s_{opt}$. The term multiplying p_3 may change sign depending on the value of the states, inputs and parameters. Nonetheless, as the states, T_{fc}, s and the current I are bounded, it is always possible to select a sufficiently small $p_3 > 0$ and a large $p_2 > 0$ to satisfy the inequality.

Moreover, once p_2 and p_3 have been fixed, $p_1 > 0$ can always be tuned such that

$$\det(\mathbf{P}) = p_1 p_3 - p_2^2 > 0, \quad \text{trace}(\mathbf{P}) = p_1 + p_3 > 0$$

which makes the matrix $\mathbf{P}$ positive definite. Finally, invoking the Finsler's lemma [10, Section 4] and the fact that the system evolves in a bounded set, we deduce the existence of a positive constants q and μ such that (4) is satisfied.

APPENDIX C
OBSERVER (5) STABILITY PROOF

Define the estimation error as $\tilde{\mathbf{x}} = \mathbf{x} - \hat{\mathbf{x}}$. Consider the system (1) and the observer (5), the error dynamics are computed as

$$\dot{\tilde{\mathbf{x}}} = \mathbf{f}(\mathbf{x}, \mathbf{u}) - \mathbf{f}(\mathbf{x} - \tilde{\mathbf{x}}, \mathbf{u}) - \kappa \mathbf{P}^{-1} \mathbf{c}^\top \mathbf{c} \tilde{x}. \tag{15}$$

where $\mathbf{u} = (I, v_{air})$. Now, by means of the mean value theorem, we are going to exploit the following identity that holds for any C^1 function $\mathbf{g}$.

$$\mathbf{g}(1) - \mathbf{g}(0) = \int_0^1 \frac{\partial \mathbf{g}}{\partial s}(s) ds.$$

Therefore, by denoting $\mathbf{g}(s) := \mathbf{f}(t, \mathbf{x} + (s-1)\tilde{\mathbf{x}})$, the following equality holds

$$\begin{aligned} & \mathbf{f}(\hat{\mathbf{x}}, \mathbf{u}) - \mathbf{f}(\mathbf{x} - \tilde{\mathbf{x}}, \mathbf{u}) \\ & \quad = \left(\int_0^1 \frac{\partial \mathbf{f}}{\partial \mathbf{x}}(\mathbf{x} + (s-1)\tilde{\mathbf{x}}, \mathbf{u}) ds \right) \tilde{\mathbf{x}}. \end{aligned} \tag{16}$$

Now, consider the following Lyapunov function candidate $V = \frac{1}{2} \tilde{\mathbf{x}}^\top \mathbf{P} \tilde{\mathbf{x}}$. The derivative of V along (15) results in

$$\dot{V} = \tilde{\mathbf{x}}^\top \mathbf{P} (\mathbf{f}(\mathbf{x}, \mathbf{u}) - \mathbf{f}(\mathbf{x} - \tilde{\mathbf{x}}, \mathbf{u}) - \kappa \mathbf{P}^{-1} \mathbf{c}^\top \mathbf{c} \tilde{\mathbf{x}}). \tag{17}$$

Recalling the equality in (16), the right-hand side of (17) reduces to

$$\begin{aligned}
&\tilde{\mathbf{x}}^\top \mathbf{P}(\mathbf{f}(\mathbf{x},\mathbf{u}) - \mathbf{f}(\mathbf{x}-\tilde{\mathbf{x}},\mathbf{u}) - \kappa \mathbf{c}^\top \mathbf{c}\tilde{\mathbf{x}}) \\
&= \tilde{\mathbf{x}}^\top \left(\int_0^1 \mathbf{P}\frac{\partial \mathbf{f}}{\partial \mathbf{x}}(\mathbf{x}+(s-1)\tilde{\mathbf{x}},\mathbf{u})ds \right)\tilde{\mathbf{x}} - \tilde{\mathbf{x}}\kappa \mathbf{c}^\top \mathbf{c}\tilde{\mathbf{x}} \\
&= \tilde{\mathbf{x}}^\top \int_0^1 \left(\mathbf{P}\frac{\partial \mathbf{f}}{\partial \mathbf{x}}((\mathbf{x}',s),\mathbf{u}) + \frac{\partial \mathbf{f}}{\partial \mathbf{x}}((\mathbf{x}',s),\mathbf{u})^\top \mathbf{P} \right. \\
&\quad \left. - \mu \mathbf{c}^\top \mathbf{c} \right) ds \tilde{\mathbf{x}} - (\kappa-\mu)\tilde{\mathbf{x}}\mathbf{c}^\top \mathbf{c}\tilde{\mathbf{x}}
\end{aligned}$$

where the compact notation $\mathbf{x}' = \mathbf{x} + (s-1)\tilde{\mathbf{x}}$ have been used. Consequently, by using (4), the following is obtained for all $\kappa > \mu$

$$\begin{aligned}
\dot{V} &= \tilde{\mathbf{x}}^\top \mathbf{P}(\mathbf{f}(\mathbf{x},\mathbf{u}) - \mathbf{f}(\mathbf{x}-\tilde{\mathbf{x}},\mathbf{u}) - \kappa \mathbf{P}^{-1}\mathbf{c}^\top \mathbf{c}\tilde{\mathbf{x}}) \\
&\leq -q|\tilde{\mathbf{x}}|^2 - (\kappa-\mu)\tilde{\mathbf{x}}\mathbf{c}^\top \mathbf{c}\tilde{\mathbf{x}} \leq -q|\tilde{\mathbf{x}}|^2. \qquad (18)
\end{aligned}$$

Next, as the proposed Lyapunov functions is upper and lower bounded as

$$\lambda_{min}(\mathbf{P})|\tilde{\mathbf{x}}|^2 \leq V \leq \lambda_{max}(\mathbf{P})|\tilde{\mathbf{x}}|^2$$

where $\lambda_{min}(\cdot), \lambda_{max}(\cdot)$ are the minimum and maximum eigenvalue, respectively, it can be shown that

$$\dot{V} \leq \frac{-q}{\lambda_{max}(\mathbf{P})} V.$$

Therefore, according to Lyapunov's second method, see, e.g. [35], the bound in (3) is satisfied.

The next step consists in showing that the observer in (5) does not have tunable settling time and is sensitive to variations in the parameters $K_i,\ \forall i \in 3,..,7$. It should be stated that, in this work, having tunable settling time and low sensitivity to parameter uncertainty means that the parameter κ of the observer (5) can be tuned to arbitrarily increase the settling time of the system or arbitrarily reduce the effect of parametric uncertainty on the estimation error. To see this fact, consider the error dynamics in (15) and the matrix $\mathbf{P}$ from the detectability condition in (4), which can be decomposed as in (14). Now, consider the following set of new coordinates:

$$\begin{bmatrix} z_1 \\ z_2 \end{bmatrix} = \begin{bmatrix} \tilde{x}_1 \\ \tilde{x}_2 + p_3^{-1}p_2\tilde{x}_1 \end{bmatrix}, \qquad (19)$$

where $\tilde{x}_1, \tilde{x}_2$ are the components of the estimation error vector $\tilde{\mathbf{x}}$. The next step consists in showing that the z_2-dynamics do not present a feedback term, thus, evolve in open-loop and are independent from κ. Specifically, the z_2-dynamics are defined as follows

$$\begin{aligned}
\dot{z}_2 &= \mathbf{f}_2(\mathbf{x},\mathbf{u}) - \mathbf{f}_2(\mathbf{x}-\tilde{\mathbf{x}},\mathbf{u}) \\
&\quad + \kappa \left(\frac{p_2}{p_1p_3 - p_2^2} - p_3^{-1}p_2 \frac{p_3}{p_1p_3 - p_2^2} \right) \mathbf{c}\tilde{\mathbf{x}} \\
&= \mathbf{f}_2(\mathbf{x},\mathbf{u}) - \mathbf{f}_2(\mathbf{x}-\tilde{\mathbf{x}},\mathbf{u}), \qquad (20)
\end{aligned}$$

where $\mathbf{f}_2$ is the second component of the vector $\mathbf{f}$. As the z_2-dynamics are independent from the feedback term, the settling time of z_2 does not depend on the value of κ. Moreover, any uncertainty in the factor $\mathbf{f}_2(\mathbf{x},\mathbf{u})$ will directly appear in the z_2-dynamics and cannot be reduced by any value of κ.

TABLE II
PARAMETERS OF THE FUEL CELL MODEL IN NUMERICAL SIMULATIONS AND EXPERIMENTAL VALIDATION

Parameter	Value (simulation)	Value (exp.)	Units
K_1	0.0025	0.0025	$K\ J^{-1}$
K_2	0.0255	0.0153	m^{-1}
K_3	$2.37 \cdot 10{-}5$	$2.37 \cdot 10{-}5$	C^{-1}
K_4	$5.33 \cdot 10^{-5}$	$5.33 \cdot 10^{-5}$	$K\ m^3\ s^{-1}J^{-1}$
K_5	$1.218 \cdot 10^{-4}$	$1.218 \cdot 10^{-4}$	$m^3\ s^{-1}$
K_6	5210	5210	K
K_7	2380	2380	atm
K_8	$3.59 \cdot 10^{-5}$	$3.59 \cdot 10^{-5}$	$J\ C\ mol^{-1}$
K_9	3.477	0.0012	$A\ m^{-2}$
K_{10}	8419	8419	K
K_{11}	0.0059	0.0059	$Pa^{-1}s^{-1}$
E_{ocv}	22.23	22.23	V
n_{cell}	20	20	$-$
T_{amb}	298	298	K
p^0	$1.196 \cdot 10^{11}$	$1.196 \cdot 10^{11}$	Pa
R_{ohm}	1	0.05	Ω
A_{geo}	0.00225	0.00225	m^2
α	1.2	1.2	$-$
s_{opt}	0.196	0.196	$-$
T_{ref}	298	298	K

APPENDIX D
OBSERVER (9) STABILITY PROOF

Define the estimation error as $\tilde{\mathbf{x}} = \mathbf{x} - \hat{\mathbf{x}}$. Consider the system (1) and the observer (9), the error dynamics are computed as

$$\begin{aligned}
\dot{\tilde{\mathbf{x}}} &= \mathbf{f}(\mathbf{x},\mathbf{u}) - \mathbf{f}(\mathbf{x}-\tilde{\mathbf{x}},\mathbf{u}) - \kappa \mathbf{P}^{-1}\mathbf{c}^\top \mathbf{c}\tilde{\mathbf{x}} \\
&\quad - \rho \mathbf{P}^{-1} \begin{bmatrix} 0 \\ 1 \end{bmatrix} (y_2 - v_{fc}(\mathbf{x}', I)) \qquad (21)
\end{aligned}$$

where $\mathbf{u} = (I, v_{air})$. Now, consider the following Lyapunov function candidate $V = \frac{1}{2}\tilde{\mathbf{x}}^\top \mathbf{P}\tilde{\mathbf{x}}$. The derivative of V along (21) results in

$$\begin{aligned}
\dot{V} &= \tilde{\mathbf{x}}^\top \mathbf{P}(\mathbf{f}(\mathbf{x},\mathbf{u}) - \mathbf{f}(\mathbf{x}-\tilde{\mathbf{x}},\mathbf{u}) \\
&\quad - \kappa \mathbf{P}^{-1}\mathbf{c}^\top \mathbf{c}\tilde{\mathbf{x}} - \rho P^{-1} \begin{bmatrix} 0 \\ 1 \end{bmatrix} (y_2 - v_{fc}(\mathbf{x}', I))). \qquad (22)
\end{aligned}$$

Therefore, according to (18), the following bound is obtained

$$\dot{V} \leq -q|\tilde{\mathbf{x}}|^2 - (\kappa-\mu)|\mathbf{c}\tilde{\mathbf{x}}|^2 - \rho(s-\hat{s})(y_2 - v_{fc}(\mathbf{x}', I)).$$

Finally, exploiting the monotonic condition in (8) and selecting $\kappa = \rho + \mu$, the next bound can be deduced

$$\dot{V} \leq -q|\tilde{\mathbf{x}}|^2 - (\kappa-\mu)|\mathbf{c}\tilde{\mathbf{x}}|^2 - \rho|s-\hat{s}|^2 = -(q+\rho)|\tilde{\mathbf{x}}|^2.$$

Therefore, similar to Appendix C, this shows that the bound in (3) is satisfied. Moreover, the convergence rate of the observer is determined by $\frac{\rho+q}{\lambda_{max}(\mathbf{P})}$, which can be arbitrarily increased by increasing ρ.

APPENDIX E
PEM FUEL CELL MODEL PARAMETERS

The fuel cell model parameters are presented in Table II.

REFERENCES

[1] J. Lai and M. W. Ellis, "Fuel cell power systems and applications," *Proc. IEEE*, vol. 105, no. 11, pp. 2166–2190, Nov. 2017.

[2] M. Jouin, R. Gouriveau, D. Hissel, M.-C. Péra, and N. Zerhouni, "Degradations analysis and aging modeling for health assessment and prognostics of pemfc," *Reliab. Eng. Syst. Saf.*, vol. 148, pp. 78 – 95, Apr. 2016.

[3] D. Zhao, F. Gao, P. Massonnat, M. Dou, and A. Miraoui, "Parameter sensitivity analysis and local temperature distribution effect for a pemfc system," *IEEE Trans. Energy Convers*, vol. 30, no. 3, pp. 1008–1018, Mar. 2015.

[4] H. Chaoui, M. Kandidayeni, L. Boulon, S. Kelouwani, and H. Gualous, "Real-time parameter estimation of a fuel cell for remaining useful life assessment," *IEEE Transactions on Power Electronics*, vol. 36, no. 7, pp. 7470–7479, 2021.

[5] B. Somaiah and V. Agarwal, "Recursive estimation-based maximum power extraction technique for a fuel cell power source used in vehicular applications," *IEEE Transactions on Power Electronics*, vol. 28, no. 10, pp. 4636–4643, 2013.

[6] K. Jiao and X. Li, "Water transport in polymer electrolyte membrane fuel cells," *Progress in Energy and Combustion Science*, vol. 37, no. 3, pp. 221–291, 2011.

[7] J. Stumper, S. A. Campbell, D. P. Wilkinson, M. C. Johnson, and M. Davis, "In-situ methods for the determination of current distributions in pem fuel cells," *Electrochim. Acta*, vol. 43, no. 24, pp. 3773–3783, Aug. 1998.

[8] A. Geiger, A. Tsukada, E. Lehmann, P. Vontobel, A. Wokaun, and G. Scherer, "In situ investigation of two-phase flow patterns in flow fields of pefc's using neutron radiography," *Fuel Cells*, vol. 2, pp. 92 – 98, Dec. 2002.

[9] I. Manke, C. Hartnig, M. Grunerbel, W. Lehnert, N. Kardjilov, A. Haibel, A. Hilger, J. Banhart, and H. Riesemeier, "Investigation of water evolution and transport in fuel cells with high resolution synchrotron x-ray radiograph," *Appl. Phys. Lett.*, vol. 90, Apr. 2007.

[10] P. Bernard, V. Andrieu, and D. Astolfi, "Observer design for continuous-time dynamical systems," *Annual Reviews in Control*, vol. 53, pp. 224–248, 2022.

[11] M. Boutayeb, H. Rafaralahy, and M. Darouach, "Convergence analysis of the extended kalman filter used as an observer for nonlinear deterministic discrete-time systems," *IEEE Transactions on Automatic Control*, vol. 42, no. 4, pp. 581–586, 1997.

[12] P. Bernard, N. Mimmo, and L. Marconi, "On the semi-global stability of an ek-like filter," *IEEE Control Systems Letters*, vol. 5, no. 5, pp. 1771–1776, Nov. 2021.

[13] J. Li, J. Klee Barillas, C. Guenther, and M. A. Danzer, "A comparative study of state of charge estimation algorithms for lifepo4 batteries used in electric vehicles," *J. Power Sources*, vol. 230, pp. 244 – 250, May 2013.

[14] M. Benallouch, R. Outbib, M. Boutayeb, and E. Laroche, "Robust observers for a class of nonlinear systems using pem fuel cells as a simulated case study," *IEEE Trans. Control Syst. Technol.*, vol. 26, no. 1, pp. 291–298, Feb. 2018.

[15] A. Pilloni, A. Pisano, and E. Usai, "Observer-based air excess ratio control of a pem fuel cell system via high-order sliding mode," *IEEE Trans. Ind. Electron.*, vol. 62, no. 8, pp. 5236–5246, Mar. 2015.

[16] A. Cecilia and R. Costa-Castelló, "High gain observer with dynamic deadzone to estimate liquid water saturation in pem fuel cells," *Revista Iberoamericana de Automática e Informática industrial*, vol. 17, no. 2, pp. 169–180, 2020.

[17] A. Cecilia and R. Costa-Castelló, "Estimation of the liquid water saturation in pem fuel cells: A low-power peaking-free dead-zone observer approach," *ISA Transactions*, 2023.

[18] J. Luna, R. Costa-Castelló, and S. Strahl, "Chattering free sliding mode observer estimation of liquid water fraction in proton exchange membrane fuel cells," *Journal of the Franklin Institute*, vol. 357, no. 18, pp. 13 816–13 833, Dec. 2020.

[19] J. Jiao and F. Chen, "Humidity estimation of vehicle proton exchange membrane fuel cell under variable operating temperature based on adaptive sliding mode observation," *Applied Energy*, vol. 313, p. 118779, May 2022.

[20] A. Cecilia, M. Serra, and R. Costa-Castelló, "Nonlinear adaptive observation of the liquid water saturation in polymer electrolyte membrane fuel cells," *Journal of Power Sources*, vol. 492, p. 229641, Apr. 2021.

[21] Y. Xing, J. Na, M. Chen, R. Costa-Castelló, and V. Roda, "Adaptive nonlinear parameter estimation for a proton exchange membrane fuel cell," *IEEE Transactions on Power Electronics*, vol. 37, no. 8, pp. 9012–9023, Aug. 2022.

[22] S. Strahl, A. Husar, P. Puleston, and J. Riera, "Performance improvement by temperature control of an open-cathode pem fuel cell system," *Fuel Cells*, vol. 14, no. 3, pp. 466–478, Mar. 2014.

[23] S. Strahl and R. Costa-Castelló, "Model-based analysis for the thermal management of open-cathode proton exchange membrane fuel cell systems concerning efficiency and stability," *Journal of Process Control*, vol. 47, pp. 201–212, Nov. 2016.

[24] T. E. Springer, T. A. Zawodzinski, and S. Gottesfeld, "Polymer electrolyte fuel cell model," *Journal of The Electrochemical Society*, vol. 138, no. 8, p. 2334, aug 1991.

[25] H. Görgün, M. Arcak, and F. Barbir, "An algorithm for estimation of membrane water content in pem fuel cells," *Journal of Power Sources*, vol. 157, no. 1, pp. 389–394, 2006.

[26] A. Husar, S. Strahl, and J. Riera, "Experimental characterization methodology for the identification of voltage losses of pemfc: Applied to an open cathode stack," *International Journal of Hydrogen Energy*, vol. 37, no. 8, pp. 7309–7315, 2012.

[27] Z. Yin, G. Li, Y. Zhang, J. Liu, X. Sun, and Y. Zhong, "A speed and flux observer of induction motor based on extended kalman filter and markov chain," *IEEE Transactions on Power Electronics*, vol. 32, no. 9, pp. 7096–7117, Sept. 2017.

[28] S. Nejad and D. T. Gladwin, "Online battery state of power prediction using prbs and extended kalman filter," *IEEE Transactions on Industrial Electronics*, vol. 67, no. 5, pp. 3747–3755, May 2020.

[29] R. G. Sanfelice and L. Praly, "Convergence of nonlinear observers on $\mathbb{R}^n$ with a riemannian metric (part ii)," *IEEE Transactions on Automatic Control*, vol. 61, no. 10, pp. 2848–2860, Oct. 2016.

[30] V. Andrieu, B. Jayawardhana, and L. Praly, "Characterizations of global transversal exponential stability," *IEEE Transactions on Automatic Control*, vol. 66, no. 8, pp. 3682–3694, Aug. 2021.

[31] S. Bonnabel and J.-J. Slotine, "A contraction theory-based analysis of the stability of the deterministic extended kalman filter," *IEEE Transactions on Automatic Control*, vol. 60, no. 2, pp. 565–569, Feb. 2015.

[32] V. Andrieu, G. Besançon, and U. Serres, "Observability necessary conditions for the existence of observers," in *52nd IEEE Conference on Decision and Control*, Dec. 2013, pp. 4442–4447.

[33] F. Barbir, *PEM fuel cells: theory and practice*. Academic Press, 2012.

[34] J. Tsinias, "Observer design for nonlinear systems," *Systems & Control Letters*, vol. 13, no. 2, pp. 135–142, 1989.

[35] H. Khalil, "Nonlinear systems, printice-hall," *Upper Saddle River, NJ*, vol. 3, 1996.